A Three-Dimensional Ankle Kinetostatic Model to Simulate Loaded and Unloaded Joint Motion

A 3D ankle kinetostatic model to simulate loaded and unloaded joint motion

Margherita Forlani

DIN-Department of Industrial Engineering

Health Sciences and Technologies,

Interdepartmental Centre for Industrial Research (HST-ICIR)

University of Bologna

Bologna, 40136 Italy

Email: margherita.forlani2@unibo.it

Nicola Sancisi

DIN-Department of Industrial Engineering

Health Sciences and Technologies,

Interdepartmental Centre for Industrial Research (HST-ICIR)

University of Bologna

Bologna, 40136 Italy

Email: nicola.sancisi@unibo.it

Vincenzo Parenti-Castelli

DIN - Department of Industrial Engineering

Health Sciences and Technologies,

Interdepartmental Centre for Industrial Research (HST-ICIR)

University of Bologna

Bologna, 40136 Italy

Email: vincenzo.parenti@unibo.it

ABSTRACT

A kinetostatic model able to replicate both the natural unloaded motion of the tibiotalar (or ankle) joint and the joint behaviour under external loads is presented. The model is developed as the second step of a sequential procedure, which allows the definition of a kinetostatic model as a generalization of a kinematic model of the joint defined at the first step. Specifically, this kinematic model taken as the starting point of the definition procedure is a parallel spatial mechanism which replicates the ankle unloaded motion. It features two rigid bodies (representing the tibia-fibula and the talus-calcaneus complexes) interconnected by five rigid binary links, that mimic three articular contacts and two nearly isometric fibers of the tibiocalcaneal and calcaneofibular ligaments. In the kinetostatic model, the five links are considered as compliant; moreover, further elastic structures are added to represent all the main ankle passive structures of the joint. Thanks to this definition procedure, the kinetostatic model still replicates the ankle unloaded motion with the same accuracy as the kinematic model. In addition, the model can replicate the behaviour of the joint when external loads are applied. Finally, the structures that guide these motions are consistent with the anatomical evidence. The parameters of the model are identified for two specimens from both subject-specific and published data. Loads are then applied to the model in order to simulate two common clinical tests. The model-predicted ankle motion shows good agreement with results from the literature.

1 Introduction

Understanding the role of the passive structures of human joints, such as ligaments, cartilage and articular surfaces, is fundamental to figuring out how these structures restrain the joint motion and how they sustain the external loads applied to the joint. In other words, it is important to understand how passive structures guarantee both the joint mobility and stability. A better comprehension of the passive structure role would help to identify articular damage in a patient, to assess the efficacy of orthopedic treatments and to design new and more effective prosthetic devices. Articular mathematical models can be useful in this context, since they make it possible to obtain data that cannot be measured on a patient, like forces exerted by ligaments and between articular contact surfaces, thus extending the present knowledge of human joints [1]. Models also have a predictive potential and could show the effects that surgical operations, prostheses, orthopedic treatments or rehabilitation have on a patient [2]. Subject-specific models are particularly suitable for these applications. Indeed, though a general description of the joint behaviour can be obtained through the use of models based on mean data, models based on anatomical data measured on a single subject provide a more accurate description of the joint behaviour for the subject itself.

The most common approach for joint modelling is the simultaneous approach, in which passive structures and muscles are considered in the model all at once. The subject-specific model parameters are identified simultaneously, trying to fit a particular motion task. Identification is generally based on optimization procedures, since it is difficult to perform based only on experimental data, given the high variability of passive structure viscoelastic properties and the difficulty to measure them on a patient [3, 4]. The simultaneous approach has been used, for instance, to define models of the knee [5] and the ankle joints [6–8], and of the entire lower limb [9]. However, this simultaneous identification does not separate the individual role that each structure has in providing both the mobility and stability of the joint. Therefore, models based on

this approach replicate a specific motion task well, but cannot accurately reproduce the behaviour of the joint in different loading conditions. To overcome this limitation, a sequential approach was proposed [10, 11]. In this case, the mobility, stability and muscle activation are sequentially analyzed in three steps, by defining three models of increasing complexity that respectively reproduce the kinematic, kinetostatic and dynamic behaviour of the joint. The kinematic model replicates the joint's natural unloaded motion and the role that passive structures have in guiding this motion. The kinetostatic model reproduces the behaviour of the joint when external loads are applied. Forces and corresponding deformations both in passive structures and in articular contacts are reproduced, so that the joint loaded motion (namely, the motion of the joint by considering deformations caused by external loads) is obtained. The dynamic model adds the muscles and their activation to sustain external loads during active loading tasks. According to the sequential approach, the model is obtained at each further step by adding articular structures and functional properties to the model of the previous step. New model parameters are identified at the corresponding step in a way that the new model performs the requested tasks, while maintaining the key features of the previous one. The functional roles of articular structures in providing mobility and stability are correctly separated and represented. In this sense, each further model represents the generalization of the previous one. The final model can replicate the behaviour of the joint in several loading conditions and, in particular, both its loaded and unloaded motion.

The sequential approach was used to model the kinetostatic behaviour of the knee joint [11]. A kinetostatic planar model of the tibiotalar joint (hereafter called ankle joint) was also defined by a sequential procedure [1]. A preliminary study on a kinetostatic spatial model of the ankle was presented in [12]. A new kinetostatic spatial model of the ankle is defined in this paper by the sequential approach, as a generalization of a previous kinematic spatial model. Tibia-fibula relative motion and talus-calcaneus relative motion are ignored. The final result is an ankle model that replicates both the unloaded (kinematic) and loaded (kinetostatic) behaviour of the tibiotalar joint. The parameters of the model are identified on two specimens, by performing an optimization based on both specimen-specific and published data. The predicted ankle motion is compared with experimental results, showing good agreement.

2 Methods

According to the sequential approach [10, 11], the new kinetostatic ankle model is defined at the second step of the procedure, by a proper generalization of a kinematic model obtained at the first step. Two basic rules are followed to preserve the function of each articular structure:

1. Parameters identified at the first step are not modified at the second step;
2. Parameters identified at the second step must not alter the results obtained at the first step.

The kinematic model only incorporates the articular structures that actually influence the joint natural kinematics. To define the kinetostatic model, new structures and viscoelastic properties are added at the second step. Thus, new parameters are introduced into the model and the identification at the second step regards only these parameters. In turn, each step is composed of a first phase of model definition (by modelling each individual involved structure) and a second phase of subject-

specific parameter identification by means of an optimization procedure. The latter can be based both on experimental and on published data. Here below, the kinematic model taken as the starting point is briefly introduced and the kinetostatic model is presented for both phases.

2.1 Kinematic model

The kinematic model replicates the behaviour of the ankle joint during passive (i.e., unloaded) motion, which is the relative motion of the tibia and talus when no external nor muscular loads are applied. The kinematic model represents the starting point for the definition of the new kinetostatic model. One of the different kinematic models of the ankle passive motion presented in the literature [13–17] is adopted in this study. In particular, the 5-5 fully parallel mechanism (5-5 FPM) with one degree of freedom (one DOF) [16] is chosen, as it proved to be a reliable model for both an accurate simulation of the one-DOF spatial (i.e., multiaxial) motion of the ankle in unloaded conditions, and a precise replication of the joint anatomical features. According to this model, the passive motion of the talus-calcaneus complex with respect to the tibia-fibula complex is guided by five structures, represented by five rigid binary links. Each link is connected to the bones by means of a spherical pair. Two binary links represent the isometric fibers (IFs) of the tibiocalcaneal (TiCaL) and calcaneofibular (CaFiL) ligaments respectively, i.e., the ligament fibers that showed an isometric behaviour during passive motion [18]. The other three links represent the three contacts between the articular surfaces of the tibiotalar joint, namely the contacts at the lateral malleolus, at the internal region of the inferior surface of the distal tibia, and at the medial malleolus. In fact, the constraint introduced by each contact is modelled as a sphere-on-sphere pair, as shown in Fig. 1(a). Each sphere-on-sphere pair is then substituted by a kinematically equivalent rigid link (called contact fiber, or CF) that connects the centres of the two spheres. As a final result, the general 5-5 FPM topology is obtained (Fig. 1(b)). This mechanism replicates the natural multiaxial motion of the ankle, i.e., three rotations and three displacements: both in the ankle and in the model, the instantaneous helical axis between the talus-calcaneus and tibia-fibula complexes does not have a fixed position or orientation from one instant to another during motion, but rotates and translates in space about and along all directions, on a well-defined path (one-DOF spatial motion).

The 5-5 FPM is defined by 35 geometric parameters: the three coordinates of the origin point $\mathbf{A}_i$ (i=1,...,5) of each binary link, represented in a reference frame connected to the tibia-fibula complex, the three coordinates of the respective insertion point $\mathbf{B}_i$ (i=1,...,5), represented in a reference frame connected to the talus-calcaneus complex, and the link length L_{0i} (i=1,...,5). These geometric parameters were identified on two specimens, to obtain two specimen-specific kinematic models. The procedure for the identification relies on experimental data and on optimization algorithms and is extensively described in [16, 19, 20]. Briefly, an experimental session was carried out in order to collect the required anatomical data on the two ankle specimens. Each specimen included the intact tibia, fibula, talus and calcaneus. The tibia was rigidly connected to a rig, while the calcaneus was free to move. The full passive dorsi/plantarflexion arc of the joint was obtained by raising and lowering a pin protruding from the calcaneus. Except for the flexion, the other five motion components (i.e., two rotations and three displacements) were unconstrained. Two trackers were fixed to the tibia and talus and their relative poses during the full range of passive dorsi/plantarflexion were collected by an optoelectronic system (Stryker Navigation System) with a nominal accuracy of 0.5° and 0.5 mm. The range of passive motion was determined by manually finding the

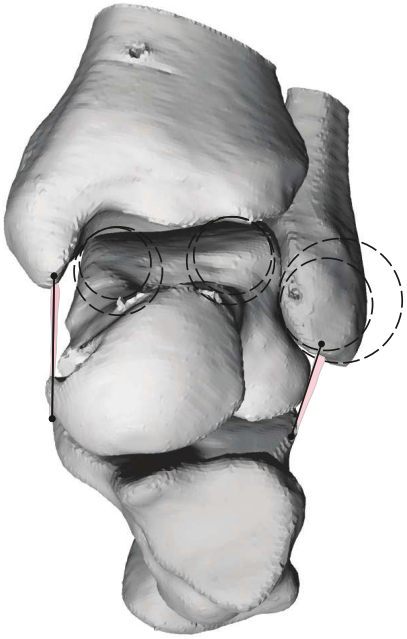

(a) The structures that guide the passive motion

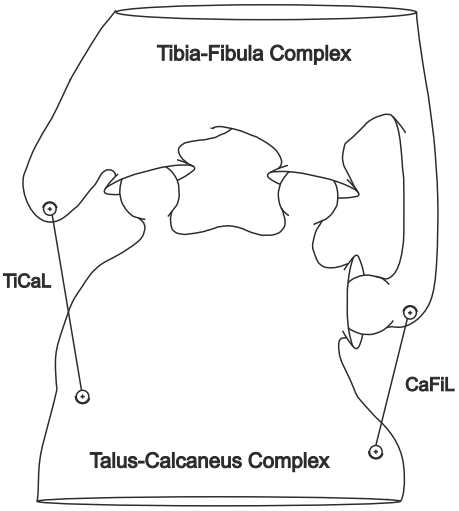

(b) The kinematic model

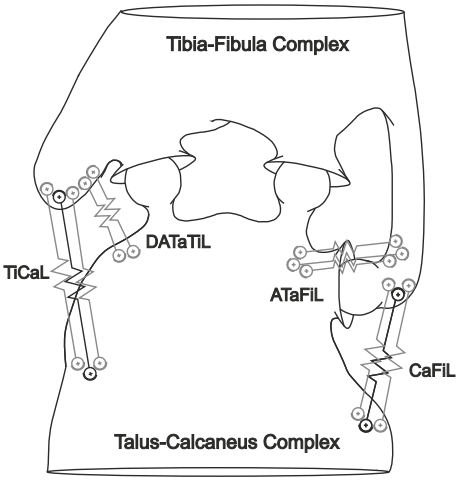

(c) Generalization from kinematic to kinetostatic model

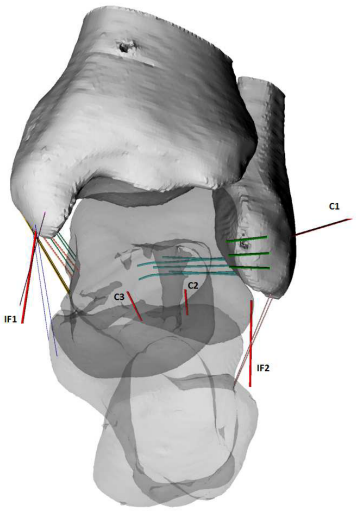

(d) The final kinetostatic model

Fig. 1. Definition of the kinetostatic model: (a) and (b) represent the definition of the kinematic model (first step of the sequential approach); (c) and (d) show the generalization of this model to obtain the kinetostatic one (second step of the procedure). In particular, the main structures guiding the passive motion are shown in (a): the three bone contacts and the TiCaL and CaFiL. A schematic representation of the kinematic model is reported in (b), where the three articular contacts are modelled as sphere-on-sphere contacts, and the two isometric fibers (IFs) of TiCaL and CaFiL are modelled by two rigid links. The IFs are considered as compliant (black lines) in (c) and elastic fibers are added (gray lines) to model other ligaments. The 26 fibers identified on the 3D bone surfaces obtained from CT scans of one representative ankle specimen are shown in (d): in particular, the IFs at the TiCaL (IF1) and CaFiL (IF2) and the CFs at the lateral malleolus (C1), at the internal region of the inferior surface of the distal tibia (C2) and at the medial malleolus (C3) are highlighted: these fibers correspond to the five constraints in (b).

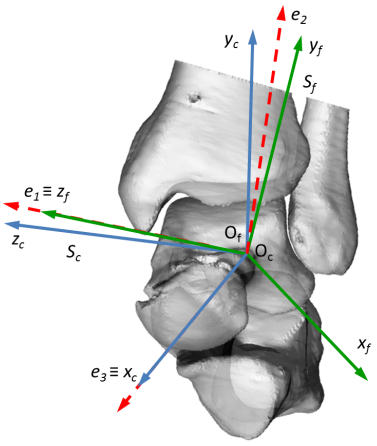

Fig. 2. The joint coordinate system used for description of the ankle motion. The reference frames S_f of the tibia-fibula and S_c of the talus-calcaneus complexes are defined according to the ISB recommendations [21]. The six components of the relative motion between the two bone complexes are described as rotations about and displacements along the axes e_1, e_2, e_3 of the joint coordinate system: axis e_1 is coincident to z_f, axis e_3 is coincident to x_c and e_2 is a floating axis perpendicular to e_1 and e_3.

two extreme flexion angles over which additional joint rotation was resisted, due to the motion constraints provided by the anatomical passive structures. For each specimen, the neutral pose of the ankle, defined as the pose of the joint where the sole of the foot and the tibia longitudinal axis are approximately orthogonal, was manually determined within the passive flexion arc by the surgeon that was present during the experimental sessions. The ankle articular surfaces and the TiCaL and CaFiL origin and insertion areas were then collected by the same optoelectronic system. CT scans were also recorded (slice increment: 0.63 mm), to define three-dimensional (3D) surfaces of the bones by segmentation that were aligned with previous data. Two anatomical reference frames, one on the tibia-fibula (S_f) and one on the talus-calcaneus (S_c) complexes, were defined according to the International Society of Biomechanics recommendations [21], as represented in Fig. 2. Each pose of S_c with respect to S_f was described by six pose components, namely three rotations (dorsiflexion(+)/plantarflexion(-), internal(+)/external(-) rotation, inversion(+)/eversion(-)) and three displacements (lateral(+)/medial(-), proximal(+)/distal(-), anterior(+)/posterior(-)) about and along three axes (respectively e_1, e_2, e_3) of the joint coordinate system defined in the same figure. Starting from the collected anatomical data, 35 provisional geometric parameters were obtained for the kinematic model of both specimens. In particular $\mathbf{A}_i$ and $\mathbf{B}_i$ were represented in S_f and S_c respectively. The parameters were then optimized for the two specimens, by minimizing the error between the pose components computed by each kinematic model, and the corresponding experimental ones. The two resulting specimen-specific models reproduce the passive motion of the two specimens.

2.2 Kinetostatic model

The kinetostatic model replicates the behaviour of the joint undergoing external loads. The kinetostatic model is obtained as a generalization of the optimal kinematic model devised at the first step of the sequential procedure. All the main passive structures of the ankle are considered, including those not directly involved in the passive motion, as they undergo elongations and exert forces to balance the applied external loads. Conversely, muscles are not included: if they are not voluntarily

activated, they have no influence on the joint response to external loads. The elastic properties of all passive structures are also considered at this step, as they affect the joint motion in loaded condition. As a result, the ankle motion is now described by a six-DOF system: the loads move the ankle motion outside the track defined by the passive motion, and the relative poses of the talus-calcaneus and of the tibia-fibula complexes depend on the external loads applied. The analysis of the role that each passive structure plays to guarantee the joint stability can thus be performed.

Specifically, all the collateral ligaments between the tibia-fibula and the talus-calcaneus complexes are considered, by adding six new ligaments besides the CaFiL and TiCaL: on the lateral side, the anterior and posterior talofibular ligaments (ATaFiL and PTaFiL); on the medial side, the ligaments that together with the TiCaL constitute the deltoid, i.e., the tibio-navicular (TiNaL), the deep anterior, deep posterior and superficial tibiotalar (DATaTiL, DPTaTiL, STaTiL) ligaments [22]. Each ligament is modelled by means of a set of elastic fibers, where each fiber represents a bundle of the respective ligament. Each fiber is a simple line element connected to the tibia-fibula and the talus-calcaneus complexes by means of spherical pairs, as shown in Fig. 1(c). Fiber-fiber interactions are not considered. Fiber-bone interactions are considered only for the PTaFiL, by means of a simplified contact model [23]. Ligament viscosity is ignored and only stiffness is considered, by modeling the elastic behaviour of each fiber. The load-elongation relationship of the j-th fiber is modelled by a function with initial quadratic toe region, passing through the axis origin and leading into a linear region at elongation ΔL_j^* [1, 24]. The linear region has slope equal to the fiber stiffness K_j and it passes through the yielding point, namely the load F_{Yj} and the corresponding elongation ΔL_{Yj} at which the ligament starts to be damaged. The function is continuous, with continuous first derivative:

$$F_j = \begin{cases} 0 & \Delta L_j \leq 0, \\ \frac{K_j}{2\Delta L_j^*}\Delta L_j^2 & 0 < \Delta L_j < \Delta L_j^*, \\ K_j\left(\Delta L_j - \frac{\Delta L_j^*}{2}\right) & \Delta L_j \geq \Delta L_j^*, \end{cases} \tag{1}$$

where F_j and ΔL_j are the load and the elongation of the j-th fiber respectively; in particular, $\Delta L_j = L_j - L_{0j}$ in which L_j and L_{0j} are the actual length and the unloaded length of the j-th fiber respectively. The percent elongation with respect to the corresponding unloaded length represents the strain of the fiber. It is possible to show that:

$$\Delta L_j^* = 2\left(\Delta L_{Yj} - \frac{F_{Yj}}{K_j}\right), \tag{2}$$

to make Eqn. (1) pass through the yielding point.

This model is applied to all considered ligaments of the ankle joint. Overall, 21 new elastic fibers (NFs) are added to those already defined in the kinematic model reported in Section 2.1 (IFs and CFs). The ligament elastic fibers are chosen as described in Tab. 1. The choice of the number of fibers for each ligament is based on the anatomical description and function

Table 1. The lateral (L) and the medial (M) ligaments and the number of fibers (NoF) used in the model.

Ligaments		**NoF**	**Anatomical information**
L	*Anterior Talofibular* (ATaFiL)	3	One fiber in the superficial bundle, one fiber in the intermediate bundle and one fiber in the deeper bundle.
	Calcaneofibular (CaFiL)	3	One anterior fiber, one posterior fiber, one IF.
	Posterior Talofibular (PTaFiL)	5	Two fibers in the deeper bundle, one fiber in the intermediate bundle and two fibers in the superficial bundle.
M	*Tibionavicular* (TiNaL)	1	One average fiber.
	Tibiocalcanear (TiCaL)	3	One anterior fiber, one posterior fiber, one IF.
	Deep Anterior Tibiotalar (DATaTiL)	2	One anterior fiber, one posterior fiber.
	Superficial Tibiotalar (STaTiL)	3	Uniformly distributed fibers along the longitudinal axis.
	Deep Posterior Tibiotalar (DPTaTiL)	3	One fiber in the deeper bundle and two fibers in the superficial bundle.

of fiber bundles [18] and on the ratio between the cross-sectional area and the length of the ligament [3, 7]. In particular, elastic fibers are added to the TiCaL and CaFiL also, to model the non-isometric bundles of these ligaments. TiCaL and CaFiL also include the IFs previously obtained at the first step of the procedure. However, the IFs are now compliant as the other fibers are.

Sphere-on-sphere pairs and the corresponding CFs allow a simple representation of the contact. In fact, contact stiffness and bone separation are taken into account by using a relationship similar to Eqn. (1) also for the CFs, but without the linear region [11]:

$$F_j = \begin{cases} 0 & \Delta L_j \leq 0, \\ K_j^{CF} \Delta L_j^2 & \Delta L_j > 0, \end{cases} \tag{3}$$

According to Eqns. (1)–(3), each ligament fiber is defined by seven geometric and three elastic parameters and each CF is defined by seven geometric and one elastic parameters. Geometric parameters are the three coordinates of the fiber origin point $\mathbf{A}_j$ in S_f, the three coordinates of the fiber insertion point $\mathbf{B}_j$ in S_c, and the fiber unloaded length L_{0j}. Elastic parameters of ligament fibers are the stiffness K_j, the yielding load F_{Yj} and the yielding elongation ΔL_{Yj}; CF elastic parameter is only the stiffness K_j^{CF}. However, the parameters that must be actually identified depend on the type of fiber, namely if it is an IF, a CF or a NF, in order to respect the rules of the sequential approach. As for the IFs, indeed, the seven geometric parameters are already defined at the first step: they are not modified in agreement with the first rule of the sequential approach. As a consequence, only the three elastic parameters have to be identified at this step for these fibers. Furthermore, also for the CFs the geometric parameters are defined at the first step, so only the stiffness K_j^{CF} needs to be identified. As for the NFs, all the geometric and elastic parameters have to be determined.

All these parameters were identified on the two specimens, to obtain two specimen-specific kinetostatic models as the

generalization of the two specimen-specific kinematic models. The procedure for the identification still relies on optimization. However, in this case the preliminary estimate of the model parameters is based both on specimen-specific experimental measures and on data from the literature: it is not possible, indeed, to measure all the parameters on a specimen. The coordinates $\mathbf{A}_j$ and $\mathbf{B}_j$ of the 21 NFs were defined on the ligament attachment areas, carefully reconstructed for each specimen on the 3D surfaces of the bones from CT scans. Published anatomical data [22, 25–28] were used as a reference during reconstruction. The geometry of the 26 fibers (21 NFs, 2 IFs, 3 CFs) of the model obtained for one of the two specimens is shown in Fig 1(d). A first estimate of the 21 unloaded lengths L_{0j} of NFs was taken as the maximum distance L_{0jm} reached between origin and insertion of the j-th fiber during the simulated passive motion. During passive motion, indeed, NFs can reach the limit between tension and no tension at most, so that the maximum elastic force associated with each fiber does not introduce significant variation in the passive motion, and IFs and CFs preserve their role in guiding it. The second rule of the sequential procedure (Section 2) is thus respected, and the replication of the passive motion by the kinetostatic model is guaranteed. The values of the ligament elastic parameters, namely K_j, F_{Yj} and ΔL_{Yj}, were taken from average data in the literature. The parameters were obtained directly from [3] for the lateral ligaments. Since the identification and classification of the medial ligaments in [3] is different with respect to the one adopted here, for the DPTaTiL and the STaTiL (considered together) the values of the posterior tibiotalar ligament were used; for the DATaTiL, the values of the tibiospring ligament were taken; the TiNaL is present also in [3], thus the reported values were used; no values are reported for TiCaL, thus the values of CaFiL were assigned to this ligament also, considering that these two ligaments have the same function in guiding the passive motion. The cross-sectional area of each ligament was divided by the number of fibers to determine the cross-sectional area of each fiber. These areas were used to assign the values of the elastic parameters to each ligament fiber consequently. Unlike the ligament fibers, the three CFs are modelled as quasi-rigid links [11]: parameters K_j^{CF} are not identified and are fixed at high values in order to simulate a rigid contact.

The loaded motion of the ankle was not measured on the two specimens and was thus taken from the literature [29] to be used as a reference for the model identification and validation. In the reference study, two loading conditions were applied to the foot by a loading rig, starting from the neutral pose: first, an inversion moment of 3.4 Nm and, second, an anterior force of 150 N, directed along a longitudinal foot axis close to axis e_3 in Fig. 2, as described in [29]. The rig was designed to not constrain the joint motion due to the external loads. These loading conditions reproduce two clinical tests commonly executed by orthopedists to control the intactness of the joint passive structures, namely the inversion and the anterior drawer tests respectively. In the reference paper, the spatial relative poses of the tibia and talus were recorded at the final position reached; the variations of the pose components from the neutral pose were calculated.

The same loading conditions were replicated in the model, in order to guarantee a significant comparison between experimental and simulated results. In particular, great attention was devoted to the external loads applied during the experimental reference tests (i.e., the foot weight and the forces related to the two tests), to their lines of action, and to their application points. Moreover, an additional pure moment about the flexion axis was applied to maintain the flexion angle at a value equivalent or close to the mean experimental value. These external loads are equilibrated by the internal reactions associated with ligament elongations and contact surface compression. In the model, these loads are obtained by Eqns. (1)–(3) for each

fiber, where the fiber elongation ΔL_j is a function of the spatial relative pose between the talus-calcaneus and tibia-fibula complexes. No further constraints are imposed on the joint motion and, as a consequence, on the elongation of each fiber: except for the flexion angle, the other five pose components (namely, the other five DOFs) are free to change according to the external loads applied. The equilibrium equations were then numerically solved to determine the spatial equilibrium pose of the talus-calcaneus complex and the variation from the neutral pose at each loading condition.

The model parameters were adjusted by a bounded optimization procedure. In particular, the 21 unloaded lengths L_{0j} of the NFs and the 23 stiffnesses K_j of all the ligament fibers (NFs and IFs) were optimized for a total of 44 parameters. The other geometric and elastic parameters were not optimized to simplify computations. The objective function f_{obj} was the mean squared weighted difference between the reference and calculated variations of the five free pose components with respect to the neutral pose, for the two considered loading conditions:

$$f_{obj} = \sum_{n=1}^{2} \sum_{h=1}^{5} \frac{\left(x_{nh} - x_{nh}^{*}\right)^2}{10\, d_{nh}^2} \tag{4}$$

where x_{nh}^{*} and x_{nh} are the reference and the relevant calculated variation of the h-th pose component (h=1,...,5) at the n-th loading condition (n=1,2) with respect to the same component in the neutral pose; the weight d_{nh} is the reference standard deviation (SD) of the variable x_{nh}.

The 44 parameters were inferiorly and superiorly bounded during optimization. The bounds for the NF unloaded lengths were:

$$L_{0j} = \left[0.98\, L_{0jm},\ 1.1\, L_{0jm}\right] \tag{5}$$

where L_{0jm} is the maximum distance reached between origin and insertion of the j-th fiber during the simulated passive motion, as defined above. The lower bounds limit the maximum strain of NFs to 2% during passive motion and, as a consequence, limit the maximum elastic force provided by each fiber in unloaded conditions: the ankle can actually be flexed with almost no external loads and the passive motion is still guided prevalently by IFs and CFs. Thus, the second rule of the sequential approach (Section 2) is satisfied. The bounds for the stiffness were:

$$K_j = \left[K_{j_{min}},\ K_{j_{max}}\right] \tag{6}$$

where $K_{j_{min}}$ and $K_{j_{max}}$ are determined considering both the SD reported in the literature and the physical meaning of Eqn. (1): by varying the stiffness, in fact, the curve can be at most completely linear or completely quadratic between the no-elongation point and the yielding point. The specimen-specific parameters of the kinetostatic model are thus obtained for each of the

two specimens.

3 Results

The elastic and geometric model parameters are reported in Tab. 2 for both specimens. The values of the 44 optimized parameters before and after optimization can be compared. No great differences are found between the preliminary estimate and optimized unloaded lengths: most of the values do not even reach the optimization bounds. Greater differences can be noted between provisional and optimized stiffness values. In particular, the greatest differences are found for some fibers of the CaFiL and for the posterior ligaments on the medial aspect in specimen A. The strain of each fiber at the neutral pose is reported in the same table, in order to facilitate comparison between the two models. A few fibers present a strain of 1%, while most of the fibers are untensioned at this pose. The greatest laxity is shown by the ATaFiL and the TiNaL in this case. The 5 fibers representing the IFs and CFs (namely, IF1, IF2, C1, C2, C3) and identified at the first step are neither tensioned or lax at the neutral pose, in agreement with the sequential procedure. It is worth noting that, for the properties of the sequential approach, the coordinates of the origin and insertion of these five fibers and their respective unloaded lengths (presented in the same table) are also the geometric parameters of the two 5-5 FPMs.

The unloaded motion of the two kinetostatic models is reported in Fig. 3: the computed motion components are compared with the relevant experimental data obtained by the optoelectronic system. The values of the root mean square (RMSE) and of the maximum (MaxErr) errors are also reported for each component. Both models replicate the experimental motion with a high accuracy. The mean values of the RMSE are 0.26° and 0.36 mm respectively for rotation and translation components over the two specimens. Maximum errors recorded were 1° and 1 mm for rotations and translations, respectively for specimen A, and were smaller for specimen B. Correlation coefficients are not computed because some motion components have a limited amplitude with respect to the nominal accuracy of experimental measurements. However, the computed and experimental curves show a similar trend. The results in loaded conditions of the two models (one for each ankle specimen) are reported in Fig. 4, where the computed pose components of the talus-calcaneus complex with respect to the tibia-fibula complex are compared with the reference data [29], for both the anterior drawer and the inversion tests. The differences with respect to the mean reference values are reported in the same figure for each component and for each specimen, both as absolute and percent values with respect to the SDs reported in the literature. Rotations and proximal/distal components present mean differences lower than the respective SDs. Greater differences are shown by anterior/posterior displacements in anterior drawer test (mean value 156% SD) and by lateral/medial displacements (mean value 106% SD). Thus, most of the model results remain inside the intervals defined by the reference SDs with only the anterior/posterior displacements in the anterior drawer test and some lateral/medial displacements falling outside these intervals.

The contribution of each anatomical structure to equilibrate the applied loads and to guarantee the joint stability was also analyzed. Almost no loads are exerted by the ligaments during passive motion, as a consequence of the lower bound imposed on the fiber unloaded lengths during optimization. The highest forces for this task are exerted at the extreme angles of dorsi/plantarflexion. The maximum force of 12 N (corresponding to a maximum strain of 0.9%) is reached at the fibers of the ATaFiL of specimen A at full plantarflexion, that results in a total force of 35 N at the whole ATaFiL ligament. At

Table 2. The geometric and elastic parameters for the 26 fibers representing the passive structures and for both specimens. For the unloaded length and stiffness, the values obtained both before and after optimization are reported. The strain of each fiber at the neutral pose is also reported. Specimen A is a right leg, specimen B is a left leg. It is worth noting that the z-axis of reference systems always points to the right [21]. Thus, for right legs, the points on the lateral and medial side of the joint have respectively positive and negative z coordinates, while it is precisely the opposite for left legs.

	STRUCTURE		FIBER	COORDINATES [mm]						UNLOADED LENGTH L_0 [mm]		STIFFNESS K_0 [N/mm]		YIELD LOAD F_Y	YIELD ELONG. ΔL_Y	STRAIN AT NEUTRAL POSE
				ORIGIN A (in S_f)			INSERTION B (in S_c)									
				x	y	z	x	y	z	BEFORE	AFTER	BEFORE	AFTER	[N]	[mm]	[%]
SPECIMEN A	L	Anterior Talofibular	ATaFiL S	13.13	17.70	20.41	20.39	8.77	13.36	26.3	26.0	51.9	51.9	96.2	1.9	-27
			ATaFiL I	12.13	15.00	22.58	18.82	5.18	15.04	24.2	23.9	51.9	51.9	96.2	1.9	-24
			ATaFiL D	11.24	13.05	24.03	18.68	2.35	15.74	23.8	23.6	51.9	51.9	96.2	1.9	-21
		Calcaneofibular	IF2	-2.55	0.95	24.32	-16.87	-24.57	20.19	19.6	19.6	38.2	63.4	119.3	3.1	0
			CaFiL A	-0.51	-0.71	33.35	-22.35	-28.37	22.07	27.0	27.7	38.2	63.5	119.3	3.1	-17
			CaFiL P	-1.86	-0.44	34.29	-23.08	-25.56	20.86	25.3	25.1	38.2	38.2	119.3	3.1	-14
		Posterior Talofibular	PTaFiL S1	-2.90	6.42	25.25	-21.61	3.85	2.46	27.7	27.4	35.0	35.0	98.7	2.8	0
			PTaFiL S2	-2.05	4.28	26.26	-21.86	1.24	1.89	29.4	29.1	35.0	35.8	98.7	2.8	-2
			PTaFiL I	-3.54	5.31	26.61	-24.05	3.21	-1.41	33.0	32.7	35.0	35.0	98.7	2.8	-1
			PTaFiL D1	-5.88	7.08	26.79	-23.47	4.45	-4.25	34.7	35.0	35.0	35.0	98.7	2.8	-2
			PTaFiL D2	-4.23	4.39	27.92	-24.55	1.23	-5.19	37.2	39.0	35.0	35.0	98.7	2.8	-8
	M	Tibionavicular	TiNaL	7.67	3.11	-36.83	55.13	-12.38	-29.19	55.6	56.5	44.0	44.0	131.5	3.0	-17
		Tibiocalcaneal	IF1	2.02	-9.94	-31.10	10.80	-21.22	-34.04	22.7	22.7	38.2	51.4	119.3	3.1	0
			TiCaL A	4.69	2.40	-36.26	6.70	-16.96	-28.13	32.5	32.8	38.2	43.3	119.3	3.1	-1
			TiCaL P	2.36	1.40	-34.65	3.29	-14.12	-29.01	28.3	28.0	38.2	38.2	119.3	3.1	-4
		Deep Anterior Tibiotalar	DATaTiL A	-4.25	4.64	-33.85	3.51	5.65	-25.17	11.6	12.0	55.3	55.3	233.3	4.2	-4
			DATaTiL P	-1.58	2.96	-33.31	5.35	6.94	-23.44	10.1	10.0	55.3	55.3	233.3	4.2	-9
		Superficial Tibiotalar	STaTiL	1.24	4.56	-40.04	-0.54	-1.85	-28.41	23.6	25.5	39.5	70.8	85.7	2.2	-9
			STaTiL	-1.66	5.26	-40.03	-4.88	-1.07	-29.03	24.3	24.6	39.5	65.7	85.7	2.2	-1
			STaTiL	-3.77	5.92	-39.94	-9.00	-0.88	-27.60	26.4	26.5	39.5	66.7	85.7	2.2	0
		Deep Posterior Tibiotalar	DPTaTiL S1	-6.23	5.30	-36.12	-7.05	4.14	-27.20	17.7	17.5	39.5	39.5	85.7	2.2	1
			DPTaTiL S2	-8.41	5.63	-33.61	-10.29	5.21	-25.82	16.9	16.8	39.5	75.2	85.7	2.2	1
			DPTaTiL D	-9.35	5.17	-36.38	-14.31	2.85	-24.76	22.5	22.3	39.5	65.2	85.7	2.2	1
	CF	Lateral Malleolus	CF1	9.52	14.73	36.70	-9.39	-6.96	46.27	13.6	13.6	-	-	-	-	0
		Troclear Surface	CF2	-4.35	-1.71	-15.65	-12.51	4.39	-25.01	15.6	15.6	-	-	-	-	0
		Medial Malleolus	CF3	3.39	-9.26	-9.26	2.14	7.23	-10.99	13.5	13.5	-	-	-	-	0
SPECIMEN B	L	Anterior Talofibular	ATaFiL S	12.77	11.34	-16.12	10.75	6.10	-14.25	20.1	20.7	47.3	42.1	74.0	2.3	-32
			ATaFiL I	11.06	8.19	-18.45	9.62	3.17	-14.62	19.4	19.2	47.3	48.2	74.0	2.3	-22
			ATaFiL D	9.11	5.23	-20.51	9.36	0.70	-14.79	19.7	19.5	47.3	63.9	74.0	2.3	-14
		Calcaneofibular	IF2	1.99	-2.21	-21.49	-18.84	-27.42	-17.24	22.4	22.4	42.2	32.9	96.3	3.4	0
			CaFiL A	2.15	0.35	-26.13	-10.52	-26.33	-14.23	23.4	23.1	42.2	32.9	96.3	3.4	0
			CaFiL P	-1.88	-0.02	-29.25	-16.85	-27.91	-13.34	24.3	26.4	42.2	38.1	96.3	3.4	-10
		Posterior Talofibular	PTaFiL S1	-3.48	7.66	-21.86	-18.80	3.84	5.18	22.5	22.9	32.9	29.2	80.0	3.3	-5
			PTaFiL S2	-4.14	4.59	-24.35	-21.04	0.34	3.82	22.2	22.0	32.9	29.1	80.0	3.3	-2
			PTaFiL I	-4.62	6.99	-23.43	-21.18	1.32	7.90	25.7	27.8	32.9	29.4	80.0	3.3	-10
			PTaFiL D1	-5.86	8.94	-22.04	-19.60	1.58	11.71	28.1	30.2	32.9	29.1	80.0	3.3	-9
			PTaFiL D2	-6.16	5.73	-24.66	-22.49	-1.77	11.79	29.8	29.5	32.9	29.1	80.0	3.3	-1
	M	Tibionavicular	TiNaL	5.75	4.34	33.59	42.98	-8.43	21.14	36.4	36.1	39.1	34.4	107.0	3.6	-22
		Tibiocalcaneal	IF1	-0.52	2.63	32.83	13.01	-12.69	30.57	22.8	22.8	42.2	32.9	96.3	3.4	0
			TiCaL A	0.80	1.84	33.53	12.77	-19.67	22.46	30.4	30.6	42.2	32.9	96.3	3.4	-5
			TiCaL P	-2.61	1.49	33.00	8.74	-16.36	25.71	25.7	25.5	42.2	32.9	96.3	3.4	1
		Deep Anterior Tibiotalar	DATaTiL A	-5.49	2.41	31.38	15.62	-2.34	18.51	16.7	16.5	61.3	40.8	175.5	4.8	-10
			DATaTiL P	-8.09	4.22	30.14	11.96	-1.13	18.10	16.5	16.4	61.3	40.8	175.5	4.8	-6
		Superficial Tibiotalar	STaTiL	-4.98	3.65	34.56	1.85	-6.00	23.17	22.2	22.0	39.1	33.6	67.5	2.5	0
			STaTiL	-7.98	4.40	33.66	-1.51	-5.50	23.88	22.6	24.6	39.1	33.6	67.5	2.5	-9
			STaTiL	-10.53	5.63	34.21	-4.93	-5.84	24.95	25.0	25.5	39.1	45.0	67.5	2.5	-3
		Deep Posterior Tibiotalar	DPTaTiL S1	-10.57	5.80	28.23	-3.68	1.91	23.40	14.8	14.7	39.1	37.9	67.5	2.5	-2
			DPTaTiL S2	-12.67	6.04	30.32	-7.17	-0.70	24.61	19.5	19.3	39.1	33.6	67.5	2.5	-1
			DPTaTiL D	-14.24	7.00	27.20	-6.16	3.04	23.98	14.1	14.1	39.1	44.5	67.5	2.5	-3
	CF	Lateral Malleolus	CF1	6.43	13.37	-24.30	-22.64	14.00	-40.24	19.9	19.9	-	-	-	-	0
		Troclear Surface	CF2	0.40	-9.10	-6.54	-1.88	-4.28	-3.45	6.0	6.0	-	-	-	-	0
		Medial Malleolus	CF3	1.58	-12.85	4.96	5.93	-5.09	8.46	7.3	7.3	-	-	-	-	0

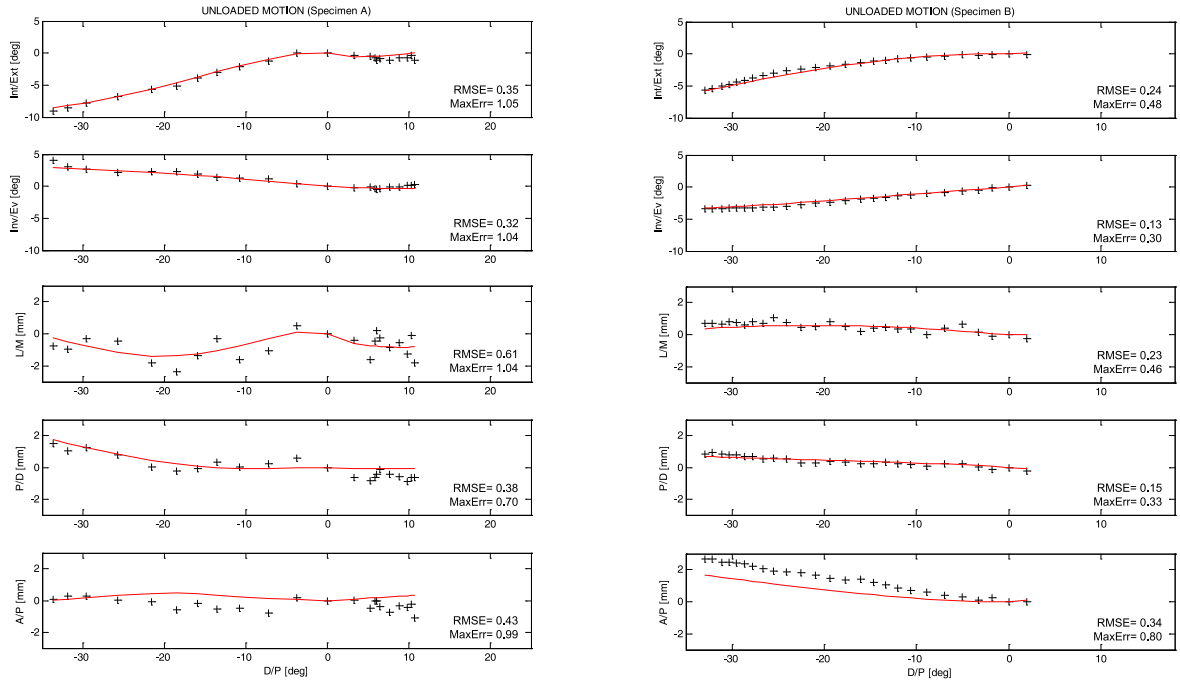

Fig. 3. Pose components of the unloaded motion for the specimens A (left) and B (right). Rotations are: D/P=dorsiflexion(+)/plantarflexion(-), Int/Ext=internal(+)/external(-), Inv/Ev=inversion(+)/eversion(-). Displacements are: L/M=lateral(+)/medial(-), P/D=proximal(+)/distal(-), A/P=anterior(+)/posterior(-). Crosses are experimental data, while continuous lines represent the model motion.

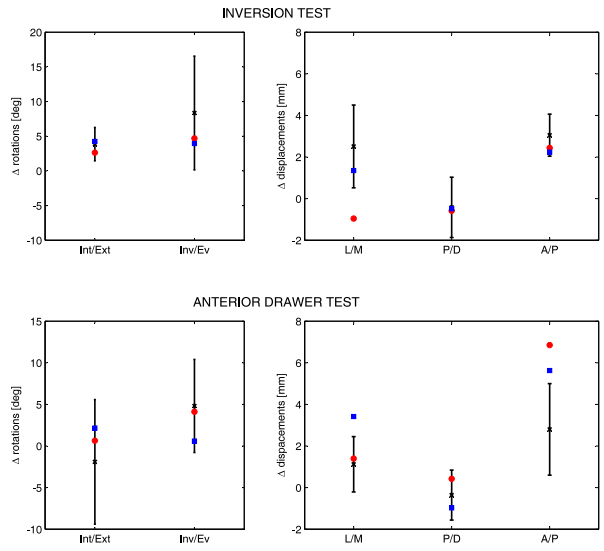

(a)

		Int/Ext	Inv/Ev		L/M	P/D	A/P
A	[deg]	-1.23	-3.67	[mm]	-3.47	-0.16	-0.61
	[%SD]	51	44	[%SD]	174	11	60
B	[deg]	0.39	-4.41	[mm]	-1.16	-0.07	-0.82
	[%SD]	16	54	[%SD]	58	5	81

		Int/Ext	Inv/Ev		L/M	P/D	A/P
A	[deg]	2.54	-0.69	[mm]	0.27	0.78	4.05
	[%SD]	34	12	[%SD]	21	65	184
B	[deg]	4.07	-4.22	[mm]	2.30	-0.61	2.83
	[%SD]	54	75	[%SD]	173	51	128

(b)

Fig. 4. Results of the two kinetostatic models determined for the specimens A (circles) and B (squares) compared with the mean values (crosses) and SDs (lines) of the reference experimental data [29]. The flexion is fixed at the mean value reported in the reference paper and the other five motion components are rotations and displacements from the neutral pose. In the tables, the absolute and relative (with respect to the corresponding SD) differences between the computed and the mean reference values of the pose components are reported.

full dorsiflexion, the highest fiber force of 9.5 N (1% of strain) is measured at the fibers of the DPTaTiL (whole ligament force of 13 N) of the same specimen. Articular contacts are important constraints for the ankle at the considered loading conditions. The contact at the lateral malleolus bears a small load (17 N) during the anterior drawer test, while it bears a load of 60 N when inversion moment is applied for specimen B. A similar behaviour is shown by the same contact for specimen A. The contact at the medial malleolus contributes in bearing the inversion moment for both specimens (forces of 69 N and 86 N for specimens A and B, respectively). Contact at the internal region of the tibia distal surface contributes in bearing the anterior drawer load for specimen B (148 N). In addition, the lateral ligaments ATaFiL and CaFiL play a crucial role in bearing both the anterior drawer force and the inversion moment. In particular, ATaFiL shows a maximum fiber strain of 6% in specimen A during the anterior drawer test and a ligament overall force of 88 N. A lower maximum fiber strain and ligament force (2.1%, 26 N) are observed for the ATaFiL fibers when the inversion moment is applied and CaFiL is involved in bearing the load, together with the already mentioned contacts. For both specimens, CaFiL provides a higher contribution in bearing inversion moments than anterior loads. In particular, for specimen B a maximum fiber strain of 8.1 and 9.6% and maximum ligament forces of 57 and 83 N are observed for anterior drawer and inversion tests respectively. The DATaTiL gives an additional important contribution during the anterior drawer test for both specimens (12.6%, 100 N in specimen A). A minor contribution is provided by TiCaL fibers (3.1%, 13 N in specimen A). These results are in agreement with other studies [18]. It must be noted that not all passive structures of the model appear to be involved in bearing the anterior drawer force and the inversion moment, in agreement with the observations reported in the literature [18].

4 Discussions

The aim of this study was to develop a kinetostatic model of the ankle joint, by means of a sequential procedure. The main characteristic of this procedure is that the kinetostatic model is defined as the generalization of a kinematic model of the ankle, that accurately replicates the joint passive motion and the structures that guide it. The generalization is performed in a way that the kinetostatic model behaviour in unloaded conditions is the same as the starting kinematic model: the unloaded motion and the role of the passive structures are preserved, so that the ankle mobility is correctly replicated. In addition, the kinetostatic model also reproduces the behaviour of the joint when external loads are applied: the ankle stability is sequentially considered. The results presented in Figs. 3–4 show that the developed model replicates quite well not only the motion of the joint in the two considered loading conditions, but also the motion when no external loads are applied to the two specimens.

The key features of the kinetostatic model and of the sequential procedure are based on the experimental evidence. In passive conditions, indeed, the unloaded motion of the ankle was shown to be mainly guided by five anatomical constraints, namely one isometric fiber of both the TiCaL and CafiL and three articular contacts [16–18, 30]. These observations are consistent with the characteristics of the ankle passive motion. Indeed, though the joint motion is complex and spatial (i.e., multiaxial), it shows one DOF [30]. From a kinetostatic point of view, a one-DOF unloaded motion can be obtained only by means of 5 simple independent constraints (in this case, three articular contacts and two ligaments). Additional constraints would reduce the number of DOFs in general: the ankle loaded motion would still be possible, but the unloaded

motion would be prevented, as external loads would be required to tighten ligaments and generate the motion itself.

These characteristics of the joint should be correctly replicated in the model in order to reproduce both the joint mobility and stability, and thus are considered by the sequential procedure. The kinematic model that is used as a starting point for the kinetostatic model definition is a 5-5 spatial parallel mechanism that features only the five structures which guide the passive motion. The model details, its anatomical significance and its accuracy were discussed in previous studies [15, 16]. It was chosen here to define the kinematic model, since it has a direct correspondence between the anatomical structures which guide the passive motion and the relevant model constraints. Moreover, it allows a high accuracy for the passive motion replication, as confirmed also in this study (Fig. 3). Most RMSE values are lower than the nominal accuracy of the measuring system (0.5°/0.5 mm). Maximum errors for specimen B are also lower than the nominal accuracy (except for the A/P displacement), while for specimen A they are higher (approximatively twice the nominal accuracy for all components except the P/D displacement) although limited to a few outliers at the extremities of the flexion arc. Some passive motion components of specimen A also appear somehow less regular and this could be due to different causes, such as friction at the articular surfaces, possible vibration of trackers, or a lower overall joint stability. Most errors of the kinematic model could thus be related to experimental inaccuracies. All the other main ankle ligaments are added during generalization from the kinematic to the kinetostatic model, but the model kinematic features are not modified so as not to alter the joint mobility: in some way, the model must still behave like a one-DOF mechanism in passive conditions, at the same time being able to behave like a compliant six-DOF system under loads, by replicating the elongations of articular structures. This means that the structures which do not guide the passive motion must be slightly tensioned at most in unloaded conditions, otherwise significant external forces would be required to stretch them and to flex the ankle, thus invalidating the concept of passive motion: there would be only one single equilibrium configuration when no external loads are applied, and not a motion path. In the model, this means that the maximum strain of the 21 NFs added at the second step must be limited during the passive motion. Obviously, the same strain should not be limited in loaded conditions, since external loads are applied in that case. These aspects are considered for the model definition to preserve the functional role of all anatomical structures both in unloaded and loaded conditions. First, the modelling of each ligament with a number of fibers allows the replication and evaluation of the different role that each ligament bundle proves to have under different loading conditions [18]. Moreover, the search domain for the unloaded lengths L_{0j} of ligament fibers is bounded during optimization (Eqn. (5)), so that a maximum strain of 2% is allowed for the NFs in unloaded conditions. The definition of this limit is important. The value considered in this study was obtained from some preliminary tests and from previous analyses on other joints, such as the knee [11]. It was then checked that each ligament fiber force corresponding to this strain were reasonably low: below 25 N for all the fibers, except for TiCaL in specimen A (45 N). In this way, the ankle can be flexed with no significant external loads, which could be involuntarily applied during passive flexion. The final optimal unloaded length for each fiber is not imposed, but adjusted by the optimization procedure within the bounds defined by this limit strain. The good results of the models are an indirect confirmation that this estimate could be reasonable. The fact that most ligament unloaded lengths do not lie on the bounds after optimization is a further confirmation. However, this limit value requires further attention and a specific investigation. For instance, the strain of some ligament fibers (and thus the relevant elastic forces) could be

theoretically higher, provided the resultant moment of all forces about the instantaneous helical axis is always almost null at all passive motion poses. This condition would be very difficult to achieve over the full flexion arc, but it cannot be completely excluded.

The geometric and elastic parameters of the model, reported in Tab. 2 for the two specimens (one left and one right ankle), were obtained by a review of the anatomical and experimental data in the literature, and by a careful reconstruction of passive structures on the 3D bone surfaces from CT scans. These data can be a reference to define either compliant models (like the one proposed in this study) or rigid body models, which in several applications, such as multibody modelling of the lower limb [16, 31], are a good compromise between accuracy and complexity. The specific characteristics of the sequential approach indeed make it possible to define the rigid kinematic model easily and directly from the geometry of the compliant kinetostatic model. Unlike other proposed models [6, 8], the relative motion between the tibia and fibula and between the talus and calcaneus are not considered in the model. This study, indeed, is focused on the modelling of the tibiotalar joint, to show the application of the sequential procedure more clearly. Nevertheless, the description of ligament structures for this joint is detailed: unlike other studies [6, 8], a multi-bundle approach is used in this case, as described above, and, for some fibers, the ligament-bone contacts are also considered. Furthermore, the constraints imposed by the fibula and the calcaneus during motion are actually included in the present kinetostatic model, but tibiofibular and talocalcaneal connections are considered rigid. For the tibiofibular motion, this assumption is justified by experimental results in the literature. The tibiofibular connection is indeed very stiff and the fibula mobility with respect to the tibia is generally low, both in loaded and unloaded conditions [18, 32], although some specimens and some loading conditions, such as ankle external rotation, could show larger fibular displacements [33]. The talus-calcaneus connection, conversely, shows a lower stiffness, especially when inversion loads are applied [34,35]. An extension of the model that considers also tibiofibular and talocalcaneal relative motions, however, can be preformed by a similar sequential procedure.

The specific procedure utilized for the development of the model allows the determination of the subject-specific parameters of a general model, via an optimization process that can be based both on experimental and published data. In particular, the procedure requires both passive and loaded motions to be used as a reference during optimization: they can be measured on a subject, or can be taken also as mean motions from the literature or from previous measurements. These motions are used together with the anatomical data measured on the specific subject (by manual palpation or medical images). In the case of this study, while the passive motion was measured on the two specimens, the loaded one was not available for the kinetostatic model and average data from the literature [29] were used as a reference. This aspect made it necessary to replicate the reported testing conditions and reference frames in the best possible way. This introduces inevitable differences and approximations with respect to the reference set-up. In particular, the representation of displacement components is highly dependent on the reference frame position in the corresponding bone complex. Displacements are represented as the relative position between two specific points of the ankle (namely the origin of S_f and S_c) during motion. This relative position is affected by the coupled ankle rotations, thus it depends on the points chosen to represent ankle displacements. Since these points in the model may not be exactly the same as in the reference data, it is not surprising that the greatest differences in loaded conditions between the model and the reference motion are found in displacement components. However, the

computed values of these components are still feasible and compatible with the normal behaviour of the ankle joint. A great variability of the anterior/posterior displacements can be found in the literature, where anterior ankle displacements during anterior drawer appear larger than those reported in the reference study [29] and closer to the results of the kinetostatic model. An anterior displacement comparable with that reported in the reference paper (about 3 mm) was obtained with an anterior force of 80 N in [36]. In the reference paper, a load of 150 N was applied, so a larger displacement would be expected. A lower stability in the anterior drawer test was reported in [37] at the whole ankle complex, where a flexibility of 0.06 mm/N was found, which would lead to a relative tibia-calcaneus displacement of 9 mm for a 150 N anterior force. However, this last study considered the whole ankle joint complex, so the motion at the subtalar joint contributed to the final displacement. In the same study [37], the flexibility at the ankle joint complex was reported for the inversion test too (8 degrees/Nm, that would lead to a total calcaneus inversion of 27.2 degrees for an inversion moment of 3.4 Nm). In this case, the greatest contribution to the total inversion rotation was noted at the subtalar joint. A smaller relative rotation was observed between the tibia and talus in [36] where a mean rotation of about 1.5 degrees was measured for an inversion load of 5.7 Nm. The inversion rotation at the tibiotalar joint computed by the two specimen-specific models is a little lower than the mean value reported in the reference paper [29], but it is still in the range defined by the SD and in agreement with the values reported in [36]. Although the model is focused on the tibiotalar joint behaviour, the approximation of the tibia-fibula and talus-calcaneus complexes as two rigid bodies is another possible source of inaccuracies. Both the talus-calcaneus and the tibia-fibula relative motion modify the relative position between the origin and insertion of some ligament fibers. Moreover, the finite stiffness of the tibiofibular connection allows additional mobility to the talus when loads are applied. This could affect the model results to different extents, particularly in those specimens or those loading conditions which show a greater either fibular or calcaneal motion, such as ankle external rotation and inversion tests. For these considerations, in spite of the accurate model validation performed in this study, specimen-specific experimental reference data would be preferred also for loaded motions, for an even better calibration of the model parameters. For instance, all 6 motion components of the considered talus-tibia relative loaded motions are reported in the reference paper, but the loads are applied starting from the neutral pose only. A more precise identification of the kinetostatic model would require that the motion of the ankle under external loads were analyzed over the full flexion arc, similarly to the identification of the kinematic model performed at the first step of the procedure.

As shown in Tab. 2, some ligaments are untensioned in passive conditions at the neutral pose. In particular, the highest laxity values are shown by ATaFiL and TiNaL for both specimens. This is consistent with the role of these ligaments, which mainly limit the plantarflexion, the anterior drawer and, as for the ATaFiL, the ankle inversion, while at unloaded neutral pose they are not tight [18]. The analysis of the fiber elongation in unloaded and loaded conditions shows that the ligament role to guarantee the joint stability is in agreement with the experimental results in the literature. Besides the crucial role of bone contacts, anterior ligaments and CaFiL contribute in bearing anterior loads, while lateral ligaments are tensioned when inversion moment is applied. Not all passive structures are involved in bearing the considered loading conditions: for instance, medial posterior ligaments are not tensioned in the two considered tasks. On the one hand, this aspect is a further validation of the model: not only is the motion replicated, but also the role of the passive structures is respected.

On the other hand, if some structures remain essentially unloaded, the identification of some model parameters could be inaccurate, since the reference motion is totally or almost insensitive to the variation of these structure parameters: small or even large variations do not affect the joint behaviour considerably. For the same reason, it is expected that the greatest differences before and after optimization could be observed for those fibers that have the largest influence on the considered motion: parameter identification for these fibers is more critical than for the others, since parameter variations have a more significant effect on the joint behaviour. This could explain the differences between the provisional and the optimal stiffness values of some fibers, such as the CaFiL, STaTiL, DPTaTiL of specimen A (Tab. 2), with respect to other fibers. However, several other factors contribute to these differences. First, the preliminary estimates of some parameters can be close to the optimal values, depending on the specimen. Moreover, the optimization bounds for the stiffness parameters depend on the SDs reported in the literature, and thus are not the same for all ligaments. Again, specific experimental tests, which make it possible to obtain all experimental data on the same specimen and in different flexion position, would help to involve all the joint anatomical structures, thus overcoming the present limits in the model validation.

5 Conclusions

A new kinetostatic model of the tibiotalar (or ankle) joint has been proposed in this study. The model is devised by a sequential procedure: a previous kinematic model of the ankle passive motion is generalized by adding ligaments and elastic properties of all the main passive structures, in order to consider their deformations and to obtain the ankle motion when external loads are applied to the joint. The scope of the model and of the sequential definition procedure is to replicate both the ankle mobility and stability, by reproducing the joint behaviour both in unloaded and loaded conditions.

The model parameters are identified on two specimens. The results of the simulations prove that, despite the great dispersions of the reference data and the overall simplifying assumptions, the model proves to be accurate both in unloaded and loaded conditions. The proposed model can be used to evaluate the behaviour of the ankle when generic external loads are applied. Furthermore, it makes it possible to analyze the contribution of the different structures to the stability of the joint. Finally, the model can be the starting point for the definition of a more complex model involving the muscle activation.

Acknowledgements

The financial support of MIUR and HST-ICIR is gratefully acknowledged. The authors also thank Dr Alberto Leardini at Istituto Ortopedico Rizzoli for the experimental facilities and for the help during experimental sessions.

References

[1] Corazza, F., O'Connor, J. J., Leardini, A., and Parenti-Castelli, V., 2003. "Ligament fibre recruitment and forces for the anterior drawer test at the human ankle joint". *Journal of Biomechanics,* **36**(3), pp. 363–372.

[2] Delp, S., Anderson, F., Arnold, A., Loan, P., Habib, A., John, C., Guendelman, E., and Thelem, D., 2007. "Opensim:

open-source software to create and analyze dynamic simulations of movement". *IEEE Transactions on Biomedical Engineering,* **54**(11), pp. 1940–1950.

[3] Siegler, S., Block, J., and Schneck, C. D., 1988. "The mechanical characteristics of the collateral ligaments of the human ankle joint". *Foot & Ankle,* **8**, pp. 234–242.

[4] Mommersteeg, T. J. A., Blankevoort, L., Huiskes, R., Kooloos, J. G. M., Kauer, J. M. G., and Hendriks, J., 1995. "The effect of variable relative insertion orientation of human knee bone-ligament-bone complexes on the tensile stiffness". *Journal of Biomechanics,* **28**(6), pp. 745–752.

[5] Guess, T. M., Thiagarajan, G., Kia, M., and Mishra, M., 2010. "A subject specific multibody model of the knee with menisci". *Medical Engineering and Physics,* **32**(5), pp. 505–515.

[6] Liacouras, P. C., and Wayne, J. S., 2007. "Computational modeling to predict mechanical function of joints: application to the lower leg with simulation of two cadaver studies". *Journal of Biomechanical Engineering,* **129**, pp. 811–817.

[7] Imhauser, C., Siegler, S., Udupa, J., and Toy, J., 2008. "Subject-specific models of the hindfoot reveal a relationship between morphology and passive machanical properties". *Journal of Biomechanics,* **41**, pp. 1341–1349.

[8] Wei, F., Hunley, S., Powell, J., and Haut, R., 2011. "Development and validation of a computational model to study the effect of foot constraint on ankle injury due to external rotation". *Annals of Biomedical Engineering,* **39**(2), pp. 756–765.

[9] Shelburne, K. B., Torry, M. R., and Pandy, M. G., 2005. "Muscle, ligament, and joint-contact forces at the knee during walking". *Medicine and Science in Sports and Exercise,* **37**(11), pp. 1948–1956.

[10] Franci, R., Parenti-Castelli, V., and Sancisi, N., 2009. "A three-step procedure for the modelling of human diarthrodial joints". *International Journal of Mechanics and Control,* **10**(1), pp. 3–12.

[11] Sancisi, N., and Parenti-Castelli, V., 2011. "A sequentially-defined stiffness model of the knee". *Mechanism and Machine Theory,* **46**, pp. 1920–1928.

[12] Forlani, M., Baldisserri, B., Sancisi, N., and Parenti-Castelli, V., 2011. "On the modelling of the ankle motion under static loads by a sequential procedure: model definition and preliminary results". In Atti del XX CONGRESSO dell'Associazione Italiana di Meccanica Teorica e Applicata, pp. 1–10.

[13] Leardini, A., O'Connor, J. J., Catani, F., and Giannini, S., 1999. "A geometric model of the human ankle joint". *Journal of Biomechanics,* **32**(6), pp. 585–591.

[14] Di Gregorio, R., Parenti-Castelli, V., O'Connor, J. J., and Leardini, A., 2007. "Mathematical models of passive motion at the human ankle joint by equivalent spatial parallel mechanisms". *Medical and Biological Engineering and Computing,* **45**(3), pp. 305–313.

[15] Franci, R., and Parenti-Castelli, V., 2011. "A one-degree-of-freedom spherical wrist for the modelling of passive motion of the human ankle joint". In *Interdisciplinary Applications of Kinematics*. Springer, pp. 183–195.

[16] Franci, R., Parenti-Castelli, V., Belevedere, C., and Leardini, A., 2009. "A new one-dof fully parallel mechanism for modelling passive motion at the human tibiotalar joint". *Journal of Biomechanics,* **42**, pp. 1403–1408.

[17] Sancisi, N., Baldisserri, B., Parenti-Castelli, V., Belvedere, C., and Leardini, A., 2014. "One-degree-of-freedom spher-

ical model for the passive motion of the human ankle joint". *Medical and Biological Engineering and Computing,* **52**, pp. 363–373.

[18] Leardini, A., O'Connor, J. J., Catani, F., and Giannini, S., 2000. "The role of the passive structures in the mobility and stability of the human ankle joint: a literature review". *Foot and Ankle International,* **21**(7), pp. 602–615.

[19] Sancisi, N., and Parenti-Castelli, V., 2010. "A 1-dof parallel spherical wrist for the modelling of the knee passive motion". *Mechanism and Machine Theory,* **45**, pp. 658–665.

[20] Parenti-Castelli, V., and Sancisi, N., 2013. "Synthesis of spatial mechanisms to model human joints". In *21th Century Kinematics*, M. McCarthy, ed. Springer, pp. 49–84.

[21] Wu, G., Siegler, S., Allard, P., Kirtley, C., Leardini, A., Rosenbaum, D., Whittle, M., DLima, D. D., Cristofolini, L., Witte, H., Schmid, O., and Stokes, I., 2002. "ISB recommendation on definitions of joint coordinate system of various joints for the reporting of human joint motion—Part I: ankle, hip, and spine". *Journal of Biomechanics,* **35**(4), pp. 543–548.

[22] Pankovich, A. M., and Shivaram, M. S., 1989. "Anatomical basis of variability in injuries of the medial malleolus and the deltoid ligament. Part 1: anatomical studies". *Acta Orthopaedica,* **50**(2), pp. 217–223.

[23] Hefzy, M. S., and Grood, E. S., 1983. "An analytical technique for modeling knee joint stiffness — Part II: Ligamentous geometric nonlinearities". *Journal of Biomechanical Engineering,* **105**, pp. 145–153.

[24] Zavatsky, A. B., and O'Connor, J. J., 1992. "A model of human ligaments in the sagittal plane. Part 2: fibre recruitment under load". *Proceedings of the Institution of Mechanical Engineers, Part H: Journal of Engineering in Medicine,* **206**, pp. 135–145.

[25] Sindel, M., Demir, S., Yildirim, A., and Ucar, Y., 1998. "Anatomy of the lateral ankle ligaments". *Turkish Journal of Medical Science,* **28**, pp. 53–56.

[26] Taser, F., Shafiq, Q., and Ebraheim, N. A., 2006. "Anatomy of lateral ankle ligaments and their relationship to bony landmarks". *Surgical and Radiologic Anatomy,* **28**, pp. 391–397.

[27] Primal Pictures, 2003. *Primal 3D Interactive series*. Primal Pictures Ltd.

[28] Netter, F. H., 2010. *Atlas of Human Anatomy*. Saunders Elsevier.

[29] Siegler, S., Udupa, J. K., Ringleb, S. I., Imhauser, C. W., Hirsch, B. E., Odhner, D., Saha, P. K., Okereke, E., and Roach, N., 2005. "Mechanics of the ankle and subtalar joints revealed through a 3D quasi-static stress mri technique". *Journal of Biomechanics,* **38**, pp. 567–578.

[30] Leardini, A., O'Connor, J. J., Catani, F., and Giannini, S., 1999. "Kinematics of the human ankle complex in passive flexion: a single degree of freedom system". *Journal of Biomechanics,* **32**(2), pp. 111–118.

[31] Moissenet, F., Chèze, L., and Dumas, R., 2012. "Anatomical kinematic constraints: consequences on musculo-tendon forces and joint reactions". *Multibody System Dynamics,* **28**(1-2), pp. 125–141.

[32] Jend, H. H., Ney, R., and Heller, M., 1985. "Evaluation of tibiofibular motion under load conditions by computed tomography". *Journal of orthopaedic research,* **3**(4), pp. 418–423.

[33] Beumer, A., Valstar, E., Garling, E., Niesing, R., Ranstam, J., Löfvenberg, R., and Swierstra, B., 2003. "Kinematics of

the distal tibiofibular syndesmosis: radiostereometry in 11 normal ankles". *Acta Orthopaedica,* **74**(3), pp. 337–343.

[34] Leardini, A., Stagni, R., and O'Connor, J. J., 2001. "Mobility of the subtalar joint in the intact ankle complex". *Journal of Biomechanics,* **34**(6), pp. 805–809.

[35] Beimers, L., Maria Tuijthof, G. J., Blankevoort, L., Jonges, R., Maas, M., and van Dijk, C. N., 2008. "In-vivo range of motion of the subtalar joint using computed tomography". *Journal of biomechanics,* **41**(7), pp. 1390–1397.

[36] Bahr, R., Pena, F., Shine, J., Lew, W. D., Lindquist, C., Tyrdal, S., and Engebretsen, L., 1997. "Mechanics of the anterior drawer and talar tilt tests: a cadaveric study of lateral ligament injuries of the ankle". *Acta Orthopaedica,* **68**(5), pp. 435–441.

[37] Lapointe, S. J., Siegler, S., Hillstrom, H., Nobilini, R. R., Mlodzienski, A., and Techner, L., 1997. "Changes in the flexibility characteristics of the ankle complex due to damage to the lateral collateral ligaments: An in vitro and in vivo study". *Journal of Orthopaedic Research,* **15**(3), pp. 331–341.